Stability analysis of an asbestos removal mobile manipulator for safe grinding trajectories

Siddharth Maraje[1], Jean-Christophe Fauroux[1], Chedli-Belhassen Bouzgarrou[1], and Lounis Adouane[2]

[1] Institut Pascal, SIGMA Clermont, Université Clermont Auvergne, CNRS, F-63000 Clermont–Ferrand, France,
siddharth.maraje@sigma-clermont.fr,
[2] Institut Pascal, Université Clermont Auvergne, CNRS, F-63000 Clermont–Ferrand, France", France

Abstract. Process of robotic asbestos removal from rehabilitation sites involves dynamic interactions between the abrasive grinding tool and the surface to be cleaned. Moreover, necessity of compact manipulator design yields a mobile base with smaller support polygon. In such case, stability becomes a critical issue. This paper presents an approach for stability estimation by analytically simulating grinding operation. Based on results of stability analysis, a grinding trajectory while ensuring manipulator stability is proposed. Analytical results are then validated through co-simulation.

Keywords: mobile manipulator, stability analysis, trajectory planning

1 Introduction and motivation

The Bots2ReC - 'Robots to Re-construction' [1] project aims towards increasing automation in the construction and demolition industry focusing on removing asbestos contamination from rehabilitation sites. Another motivation is to avoid human operators from undertaking the dangerous task of manual asbestos removal. In [2], asbestos removal use case and cleaning scenario are explained in detail. For the project Bots2ReC, targeted cleaning sites include medium and small sized rooms (typically, offices or flats). Thus, the application scope is much beyond a system for asbestos removal from pipes presented in [3].

1.1 Problem identification

Asbestos removal use case. Since asbestos removal process includes grinding hard contaminated materials like plaster, resurfacing concrete and tiles etc. (from walls, ceiling and floor) high reaction forces are generated in the process. By anticipating complexity involved in controlling the task, it was proposed to perform grinding by fixing the pose of the mobile base. Consequently, time taken for base repositioning remains idle (non-productive). Thus, to reduce number of base placements and the resulting idle time, it is necessary to access area, as large as possible at a given position of the mobile base. A critical constraint of stability however, appearing due to changing arm configuration, presence of arm dynamics and reaction wrench from grinding process, tends to limit the accessible area. Moreover, to yield a time efficient operational process, emphasis is to perform removal operation at optimal grinding parameters for a given material namely, depth of cut (d), linear grinding velocity (V) etc. Since these process parameters determine the magnitude of reaction wrench, it is necessary to develop a systematic methodology of stability evaluation of mobile manipulator under the effect of aforementioned factors and hence a stable cleaning area accessible at given base position.

In literature, stability of the mobile manipulators has been mostly addressed for issues like planning trajectory of the mobile base inside work-environment, determining it's load carrying capacity and safe navigation [5][6][7]. Since the use of robotic systems in construction industry is not prevalent, study of stability of machining mobile manipulator operating under dynamic process parameters and having compact support polygon is not common. Also, association of manipulator stability with arm motion planning for machining processes is not widely studied. A methodology for dimensional synthesis of a robotic arm was demonstrated in [8] under constraints of overall dimensions and weight of the mobile manipulator, collision avoidance and requirement of maximizing reachable surface area at a given base position. Critical cleaning scenario were analyzed to identify 7-dof redundant arm (6R arm mounted on a vertical slider) as a suitable architecture. This approach helped in obtaining optimal base placement with respect to cleaning surface.

In this paper, the work of [8] is continued by proposing a systematic methodology for stability evaluation. Here, we focus on the grinding of walls. The organization of the paper is as follows. Section 2 describes two approaches of stability estimation i.e. analytical and co-simulation. Sections 3 and 4 present structural and dynamic stability analysis to identify stable cleaning zones. Section 5 demonstrates a stable cleaning trajectory based on the previous analysis and the paper is concluded in section 6.

2 Methodology for stability evaluation

Fig. 1 shows mobile manipulator placed at a distance b from wall surface (S). At this distance, the 3D workspace (W) of the robotic arm intersects with surface (S) in circle (C). Area included by the C is the area available for cleaning at a given base placement such that collision free (arm-cleaning environment) continuous trajectories are feasible. However, since the robotic arm is mounted on a vertical slider, the circle C can be displace on a vertical axis to result a workspace with geometric shape called 'stadium' (rectangle with semicircles on either of the opposite sides).

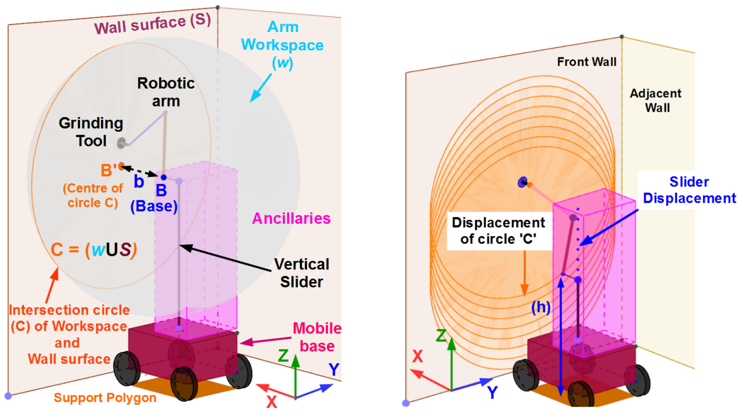

(a) Representation of workspace (b) Extension of workspace

Fig. 1: Representation of asbestos use case scenario using Geogebra [4]

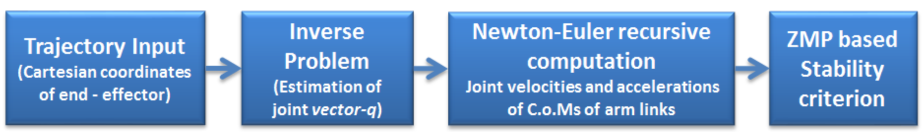

Fig. 2: Analytical approach for ZMP estimation

2.1 Analytical method

Analytical estimation of stability is performed using MATLAB simulation. Fig. 2 shows estimation of stability using analytical approach. Functionalities provided by Peter Cork's Robotic toolbox [9] are used to define geometry of the robotic arm, define inertial parameters (C.O.Ms, mass, inertia matrix) and find accurate inverse geometric solution. Coordinates of end-effector serve as an input to the model. ZMP (zero moment point) is defined as a point on the ground at which the net moment of the inertial forces and the gravity forces has no component along the horizontal axes [11]. The two components of ZMP are presented as:

$$x_{zmp} = \frac{\sum_{i=1}^{n} m_i(\ddot{z}_i + g)x_i - \sum_{i=1}^{n}(m_i\ddot{x}_i)z_i - \sum_{i=1}^{n}(T_y)_i}{\sum_{i=1}^{n} m_i(\ddot{z}_i + g)} \tag{1}$$

$$y_{zmp} = \frac{\sum_{i=1}^{n} m_i(\ddot{z}_i + g)y_i - \sum_{i=1}^{n}(m_i\ddot{y}_i)z_i - \sum_{i=1}^{n}(T_x)_i}{\sum_{i=1}^{n} m_i(\ddot{z}_i + g)} \tag{2}$$

where, i indicates number of rigid bodies, (x_i, y_i, z_i) indicate coordinates of the C.o.M of the i^{th} body and (T_x, T_y) indicate components of derivatives of angular momentum, where, $T_i = I_i\dot{\omega} + \omega_i \times I_i\omega_i$.

Newton-Euler recursive formulation is used to compute joint velocities (ω) and accelerations $(\dot{\omega})$ of moving bodies. Forces occurring during grinding operation: normal reaction force (F_N), tangential reaction force (F_T) and (R) reaction torque acting in a direction opposite to that of the tool rotation are shown in Fig. 3. Direction of reaction wrench in the global reference frame 'XYZ' depends on the direction of tool rotation and tool advancement as well as the surface being cleaned (front wall or side wall shown in Fig. 1). Accordingly, we have $F_T = [F_{T_x} F_{T_y} F_{T_z}]$, $F_N = [F_{N_x} F_{N_y} F_{N_z}]$ and $R = [R_x R_y R_z]$ where, subscripts x, y and z indicate components in global coordinate frame. From the definition of ZMP, we see that each term in the numerator represents a moment acting on the system. Thus, to integrate grinding forces within ZMP, moments produced by these forces must be taken into account. Fig. 3 shows distances z_n along Z-axis and x_t along X-axis, responsible to create moments due to forces F_{N_x} and F_{T_z} respectively. Incorporating these moments, Eq.1-2 can be re-written as,

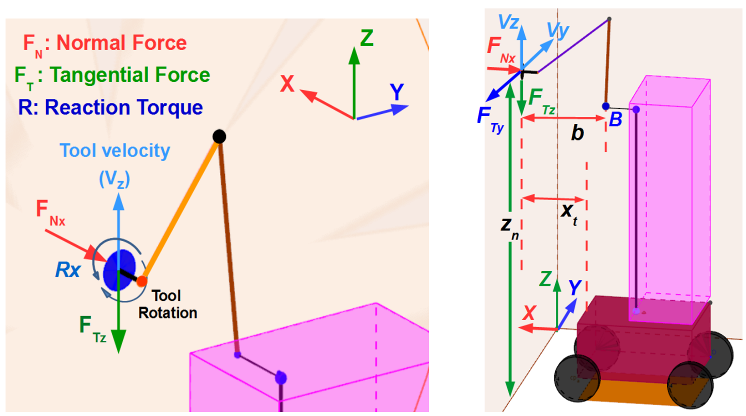

(a) Reaction forces (b) Moments

Fig. 3: Forces and moments acting during grinding operation [4]

$$x_{zmp} = \frac{\sum_{i=1}^{n} m_i(\ddot{z}_i+g)x_i - \sum_{i=1}^{n}(m_i\ddot{x}_i)z_i - \sum_{i=1}^{n}(T_y)_i - M_{F_N x} \pm M_{F_T x} \pm Rx}{\sum_{i=1}^{n} m_i(\ddot{z}_i+g)} \quad (3)$$

$$y_{zmp} = \frac{\sum_{i=1}^{n} m_i(\ddot{z}_i+g)y_i - \sum_{i=1}^{n}(m_i\ddot{y}_i)z_i - \sum_{i=1}^{n}(T_y)_i - M_{F_{N_y}} \pm M_{F_{T_y}} \pm Ry}{\sum_{i=1}^{n} m_i(\ddot{z}_i+g)} \quad (4)$$

where, M_{F_N} and M_{F_T} are a moments due to normal and tangential reaction forces F_N and F_T, $M_{F_N} = [M_{F_{N_x}} M_{F_{N_y}} M_{F_{N_z}}]$, $M_{F_T} = [M_{F_{T_x}} M_{F_{T_y}} M_{F_{T_z}}]$ and $R = [R_x R_y R_z]$.

2.2 Method of co-simulation

A dynamic simulation environment is constructed in ADAMS software. It consists of a multi-body dynamic model of the mobile manipulator with ground-ceiling-wall as a cleaning environment. Components of the mobile manipulator are indicated in Fig. 4. Inputs to ADAMS model are joint torques required to generate given trajectory whereas outputs retrieved from the model are linear and angular joint velocities, joint accelerations and C.O.Ms of moving bodies. ZMP is then estimated using Eq. (3) and (4). A strong dynamic engine of ADAMS is helpful in verifying analytical results obtained through analytical method.

Table 1: MDH parameters

Link (i)	θ	d	α	a
1	0	d_1^*	0	0
2	q_2	0.1	$\frac{pi}{2}$	0.157
3	q_3	0.6	0	0.6
4	q_4	0	$\frac{-pi}{2}$	0
5	q_5	0	$\frac{pi}{2}$	0
6	q_6	0.13	$\frac{-pi}{2}$	0.13
7	q_7	0	0	0

$^*d_1 = h = [0.5, 1.8]\, m$

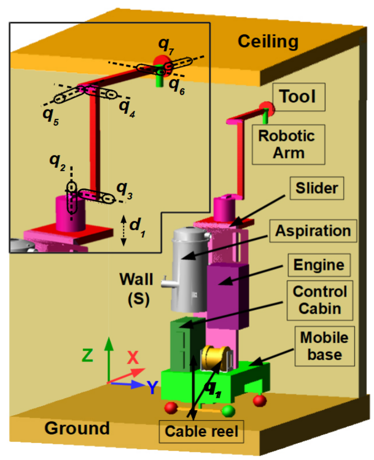

Fig. 4: Multibody dynamic model

3 Evaluation of structural stability

Structural stability analysis evaluates reachability of the manipulator in quasi-static state over circle C for no-contact condition with the wall. Table (1) presents Modified Denavit-Hartenberg (MDH) parameters of the robotic arm [10]. For performing collision free continuous grinding trajectories, base 'B' of the mobile manipulator is placed at $b = 0.75\, m$ from the wall (S). Resultant circle of intersection C has a diameter of 1.8 m. Further, to be able to interpret ZMP as a stability margin, we convert ZMP coordinates to percentage stability. In our case, mobile base has a support polygon '$S_1S_2S_3S_4$' of dimensions $(600 \times 457)\, mm$ with lateral and longitudinal axes 'Y_L-Y_R' and 'X_F-X_R' respectively (see Fig.5). The polygon is divided in four quadrants namely, front-left (F_L), front-right (F_R), rear-left (R_R) and rear-right (R_R). Longitudinal (S_{long}) and lateral (S_{lat}) percentage stability of point 'i' having ZMP coordinates (x_i, y_i) is calculated as,

$$S_{long} = \left(\frac{min(d_{XF}, d_{XR})}{0.5 \times l}\right) \times 100, \quad S_{lat} = \left(\frac{min(d_{YR}, d_{YL})}{0.5 \times w}\right) \times 100 \tag{5}$$

where, $d_{XF} = \left|\frac{l}{2} - x_i\right|$, $d_{XR} = \left|\frac{l}{2} + x_i\right|$, $d_{YL} = \left|\frac{w}{2} - y_i\right|$, $d_{YR} = \left|\frac{w}{2} + y_i\right|$

Circle C is discretized in polar coordinates, r [0, 0.9] and θ [0, 2π] (see Fig.6).

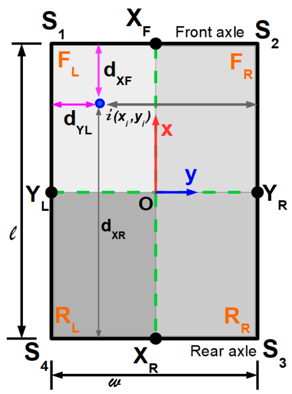

Fig. 5: Notations for stability in the support polygon

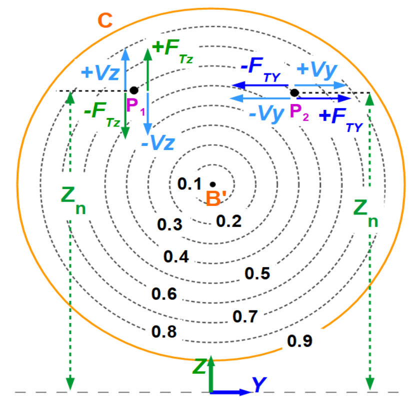

Fig. 6: Discretization of workspace and direction of tangential reaction forces

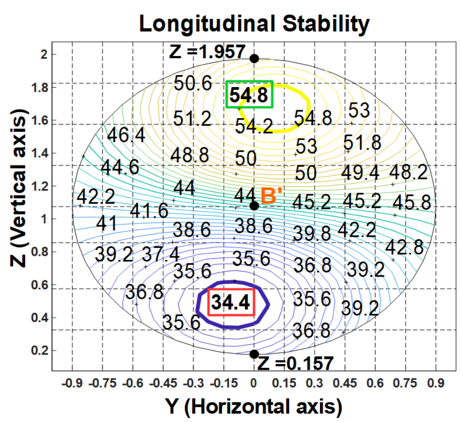

Fig. 7: Longitudinal structural stability

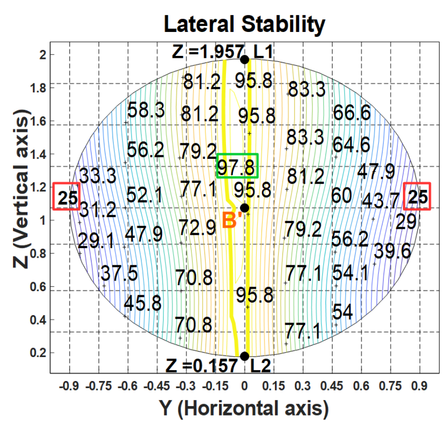

Fig. 8: Lateral structural stability

Percentage longitudinal and lateral stabilities for each pose of the manipulator inside circle C are shown in Fig. 7 and Fig. 8. Here, slider height $h = 0.9\,m$ and point B'(0, 1.057) is the center of circle C in Fig. 6. Longitudinal stability is highest (55%) near (0.1, 1.675) i.e 0.6 m above point B' and lowest (34%) near (-0.1, 0.457) i.e 0.6 m below point B'. Top to bottom, longitudinal stability decreases. Lateral stability has a symmetric variation about vertical axis passing through Y = -0.05 m (see Fig. 8). This lateral shift is due to unbalanced component integration on the mobile base. Except for axis of symmetry (LL'), along any vertical line inside C, lateral stability decreases from top to bottom. This is the result of increase in the overhanging distances of arm links from top to bottom. Near Y = 0.9 m and -0.9 m blue zones indicate decrease in stability close to 25%.

4 Evaluation of Dynamic stability

For grinding wall surfaces, a minimum normal force of around 80 N is applied by the tool on cleaning surface. A tangential reaction force of maximum magnitude 120 N is seen to be generated due to cutting geometry and tool translation along with reaction force of 80 N. These values are determined from the preliminary experimental investigation conducted under the project.

Referring to Fig. 3, F_{Nx} is the normal reaction force acting along -X direction at distance z_n along Z-axis producing a moment ($M_{F_{Nx}}$=-$F_{Nx} \times z_n$). Direction of tangential force F_T depends on the direction of tool velocity. According to Fig. 6, for $+V_z$ and -V_z velocity of P_1, tangential forces are -F_{Tz} and $+F_{Tz}$ while momets are -$M_{F_{Tz}}$ and $+M_{F_{Tz}}$ respectively. From Eq. 3, it can be concluded that $+M_{F_{Tz}}$ tends to push ZMP towards the edge S_1S_2 of the polygon and hence reduce longitudinal stability. Thus, investigating the case where tool has velocity $+V_z$ is necessary. Each point P_i (r, θ) on circle C is displaced by a disance 0.001 m along +Z and +Y with an acceleration of 0.1 m/s^2. These value are arbitrarily chosen to evaluate behaviour of the system when subjected to acceleration. Longitudinal stability for vertical motion and lateral stability for horizontal motion are then evaluated for two slider heights (h=0.9 and 1.8 m).

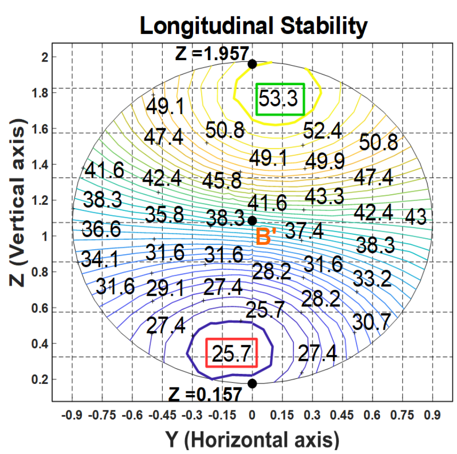

Fig. 9: Longitudinal stability at h = 0.9m, Y[-0.9, 0.9], z_n[0.175, 1.975]

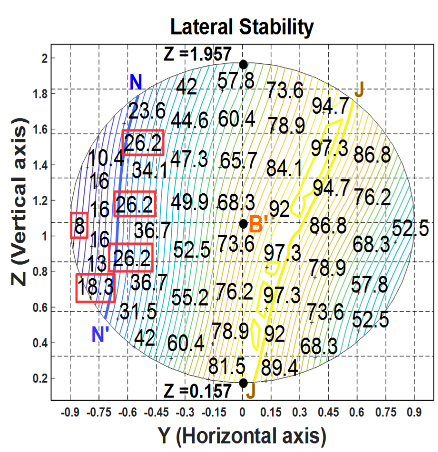

Fig. 10: Lateral stability at h = 0.9m, Y[-0.9, 0.9], z_n[0.175, 1.975]

Fig. 9 and Fig. 11 show longitudinal stability over C when h=0.9 and 1.8 m respectively. Difference in stability values is observed due to change in tool altitude z_n. For example, the lowest value of stability is reduced to 25% near z_n=0.457 m (i.e. 0.6 m below B') in Fig. 9. Where as in Fig. 11 the lowest value is 32% at z_n=1.357 m (0.6 m below B'). Thus, higher the value of z_n higher is the moment ($M_{F_{Nx}}$) and higher the stability. This explains change in the highest value of longitudinal stability in two cases. In fig. 10, line NN' passing through

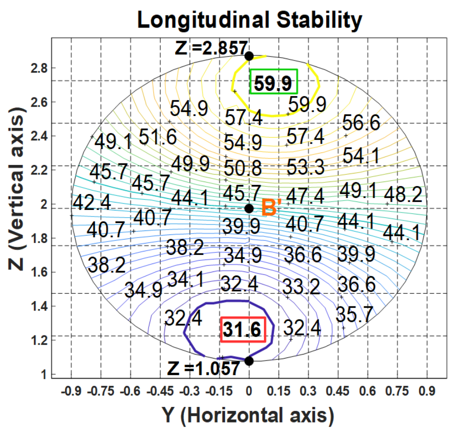

Fig. 11: Longitudinal stability at h = 1.8m,Y[-0.9, 0.9], z_n[0.175 2.875]

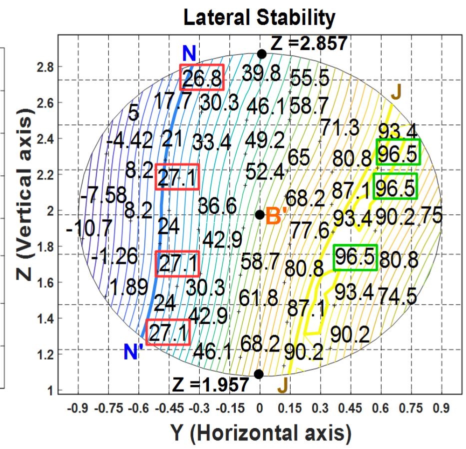

Fig. 12: Lateral stability at h = 85m, Y[-0.9, 0.9], z_n[0.175, 2.875]

points (-0.75, 0.6) and (-0.55, 1.8) indicates a stability line of 26%. Here an important point to note is, since tool is moving in +Y, tangential force F_{Ty} acts along -Y at a distance of z_n. Thus, stability is critical between NN' and Y = -0.9 m. It improves along +Y direction and gets maximum at JJ'. At Y = 0.9 m, in spite of tool being at the boundary of the workspace, stability is not critical since the moment ($M_{F_{Ny}}$ = -$F_{Ny} \times z_n$) now tends to increase the stability. In fig.12 negative stability indicates ZMP outside support polygon. Stability line NN' is shifted to pass through points (-0.6, 1.3),(0.28,0.35) decreasing stable zone inside C compared to that in Fig. 10. This shift is observed due to loss of stability caused by higher value of ($M_{F_{Ny}}$) due to higher z_n. Thus, an important conclusion is that, while moving along Y direction, a movement away from Y= 0 axis results in stable pose due to tangential reaction force acting towards 'Y = 0' axis. In Fig. 13, Pose 1 indicates arm configuration when stability is maximum (60% in Fig. 11). Pose 2 indicates arm configuration at lowest stability value (31.6% in Fig. 11) and Pose 3 indicates lateral arm configuration where, structural stability (Fig. 8) is critical.

Stability based trajectories. Asbestos removal grinding trajectories are illustrated based on the conclusions of stability analysis. Since, most cleaning walls are rectangular in shape, we assume a rectangle of dimensions $(1.38 \times 1.13)\,mm$ inside C. A boustrophedon path [12] is tracked separately from point S to E_1 and S to E_2 instead of one single path from E_1 to E_2. The tool motion along -Y while cleaning inside Y< 0 zone and along +Y while cleaning inside Y> 0 zone results in a stable manipulator operation. Fig. 15 shows variation of ZMP obtained by matlab simulation and co-simulation during the two grinding trajectories. It can be safely concluded that analytical model can be trusted for simulating grinding trajectories in future.

Table 2: Inertial properties of links

Link (i)	Mass (Kg)	Principle Inertias ($Kg.m^2$)
1	10	$[0.19 \quad 0.1 \quad 9.8\times10^{-2}]$
2	30	$[0.156 \quad 0.146 \quad 0.11]$
3	25	$[0.836 \quad 0.836 \quad 6.65\times10^{-3}]$
4	2	$[2.74 \quad 2.73 \quad 0.516]\times10^{-3}$
5	20	$[0.67 \quad 0.67 \quad 5.3\times10^{-3}]$
6	5	$[0.102 \quad 8.08 \quad 3.28]\times10^{-3}$
7	20	$[1.96 \quad 1.01 \quad 1.01]\times10^{-2}$

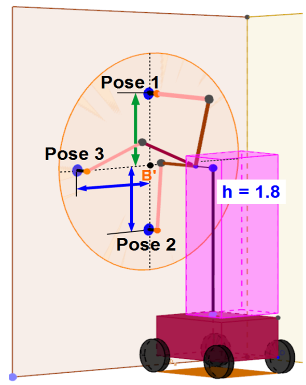

Fig. 13: Stability Poses

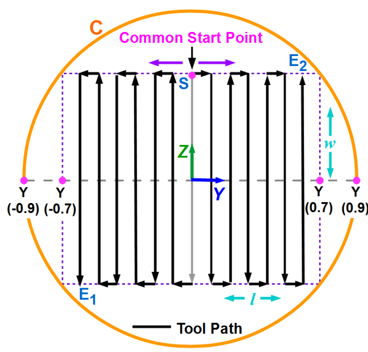

Fig. 14: Path traced by tool on the wall

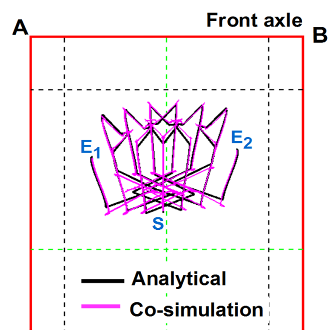

Fig. 15: ZMP estimation through analytical and co-simulation

5 Conclusion and future work

In this paper, a methodology for simulating robotic asbestos removal under constraint of stability was presented. Since, mobile manipulator has a constraint of keeping it's base fixed while performing grinding operation, stability becomes a critical issue to tackle. Analytical approach for estimating stability and hence cleaning zones for stable manipulator operation were identified for two different slider positions. By identifying the effect of normal and tangential reaction forces on the stability of the mobile manipulator, it was possible to propose a grinding trajectory that covers maximum area inside cleaning workspace (C). Finally the analytical approach was validated through co-simulation. In future, the validity of analytical approach will enable performing rapid stability evaluation for different cleaning scenarios e.g. ceiling, floor and curved surfaces compared to a prolonged time taken by co-simulation (ADAMS-MATLAB). Also, the stability based area partitioning for grinding entire wall or ceiling surface by repositioning mobile base is a potential future work.

Acknowledgment Bots2ReC project is funded by the EU H2020 research and innovation program (Grant agreement No: 687593).

References

1. Bots2ReC Homepage, https://www.bots2rec.eu, last accessed 2018/10/25
2. Detert, T., Charaf Eddine, S., Fauroux, JC. et al: Bots2ReC: introducing mobile robotic units on construction sites from asbestos rehabilitation. Construction Robotics (1), 29-37 (2017).
3. Arai, M., Hoshino, H., Robot system for removing asbestos sprayed on beams. In: 28th International Symposium on Automation and Robotics in Construction (ISARC), pp. 1409 - 1414. Seoul, Korea (2011),
4. Geogebra Homepage, https://www.geogebra.org, last accessed 2018/11/12
5. Huang, Q., Tanie, K., Sugano, Shigeki.: Coordinated motion planning for a mobile manipulator considering stability and manipulation. International journal of robotics research (19), 732 (2000)
6. Korayem, M., Azimirad, V., Nikoobin A., Bouroujeni, Z.: Maximium load-carrying capacity of autonomous mobile manipulator in an environment with obstacle considering tip over stability. International journal of advanced manufacturing technology (46), 811-829.
7. Khalil, A., Daemi, P., Hassanpour, A., Tarvirdizadeh, B.: On the capability of wheeled mobile robots for heavy object manipulation considering dynamic stability constraints. Multibody system dynamics (41:2), 101-123 (2017)
8. Maraje, S., Fauroux, J-C., Dimensional synthesis of a robotic arm for mobile manipulator using an interactive geometric software. In: Proceedings of The 12th IFToMM International Symposium on Science of Mechanisms and Machines, pp 253-261. Iasi, Romania (2017)
9. Corke, P.: Robotics, Vision & Control: Fundamental Algorithms in Matlab, Springer, 2011.
10. Khalil, W., Dombre E.: Modeling, Identification and Control of Robots, CRC Press, 2002.
11. Vukobratovic, M., Juricic, D., Contribution to the synthesis of biped gait, In: Proceedings of IFAC Symposium on Technical and Biological Problems on Control, Erevan, USSR, (1968)
12. Choset H., Pignon, P., Coverage path planning: The boustrophedon cellular decomposition, in International Conference on Field and Service Robotics, Canberra, Australia, (1997).